Electronic Supplementary Material (ESI) for Biomaterials Science.

Supporting Information

Chloroplast-inspired Nanoplatform for Targeting Cancer and Synergistic Photodynamic/Photothermal therapy

Zhengxi Guo, Xiaohong Zhou, Cheng Hou, Zhaoyang Ding, Changchun Wen, Lai-Jun Zhang, Bang-Ping Jiang, and Xing-Can Shen*

State Key Laboratory for Chemistry and Molecular Engineering of Medicinal Resources, School of Chemistry and Pharmaceutical Science, Guangxi Normal University, Guilin, 541004, P. R. China.

*Corresponding author. Email: xcshen@mailbox.gxnu.edu.cn

Table of Contents

Fig. S1. The Structure of Cu(II)Chl, PEG-Diamine, HA. S1

Fig. S2. Conjugation efficiency of Cu(II)Chl into Cu(II)Chl-HA NPs. S2

Fig. S3. Concentration-dependent absorbance curve. S3

Fig. S4. TEM Diameter Distribution of Cu(II)Chl-HA NPs. S4

Fig. S5. DLS results of Cu(II)Chl-HA NPs. S5

Fig. S6. Digital photographs of Cu(II)Chl-HA in different media. S6

Fig. S7. Time-dependent absorption spectra of Cu(II)Chl-HA in different media. S7

Fig. S8. Time-dependent average hydrodynamic size plots of Cu(II)Chl-HA in different media. S8

Fig. S9. Frontier molecular orbital distribution. S9

Table S1. Triplet and singlet excitation energy. T1

Fig. S10. ROS evaluation by DPBF method. S10

Fig. S11. $^1O_2$ generated investigation. S11

Fig. S12. Cellular uptake assay by ICP-OES. S12

Table S2. Literature comparation of light power for photodynamic therapy. T2

Fig. S13. Plots of Cu contents into Cu(II)Chl-HA NPs. S13

Fig. S14. Digital IR thermal imaging in vivo. S14

Fig. S15. Digital photograph of harvested tumors. S15

Fig. S16. Average weight changing curve. S16

Fig. S17. Histological H&E staining assay. S17

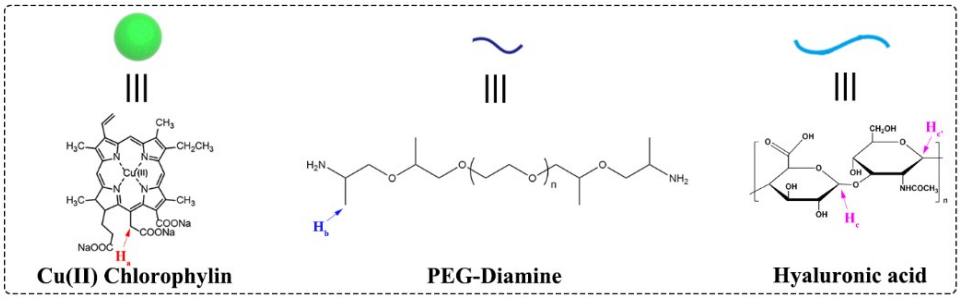

Fig. S1. The chemical structure of Cu(II)Chlorophylin, PEG-Diamine, HA, insert: corresponding typical characteristic proton.

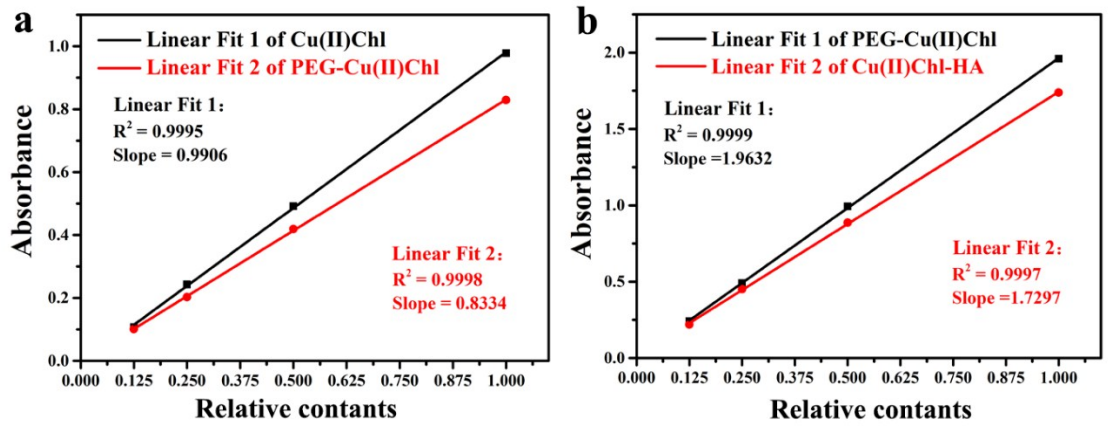

Fig. S2. Conjugation efficiency of Cu(II)Chl into Cu(II)Chl-HA NPs, (a) the absorbance of reactant (sodium Cu(II)Chl) and product (PEG-Cu(II)Chl) in accordant dilute aqueous condition, (b) the absorbance of reactant (PEG-Cu(II)Chl) and product (Cu(II)Chl-HA) in accordant dilute aqueous condition.

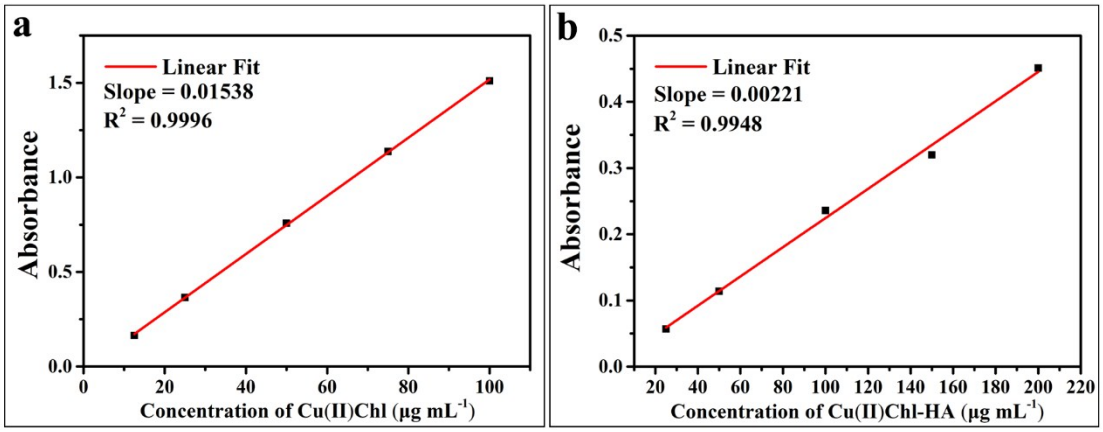

Fig. S3. Concentration-dependent absorbance standard curve of (a) Cu(II)Chl and (b) the Cu(II)Chl-HA NPs**.**

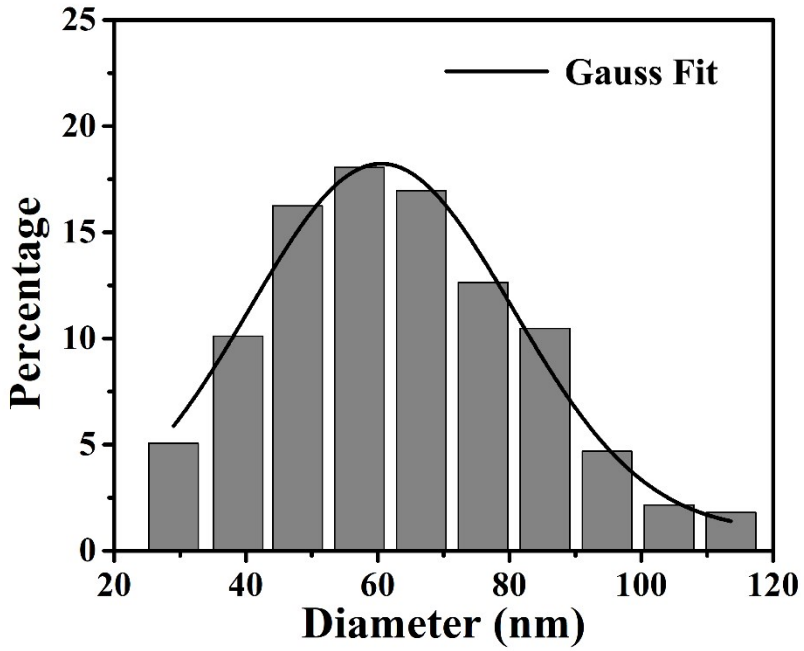

Fig. S4. Corresponding TEM diameter distribution of Cu(II)Chl-HA NPs with gauss fitting curve.

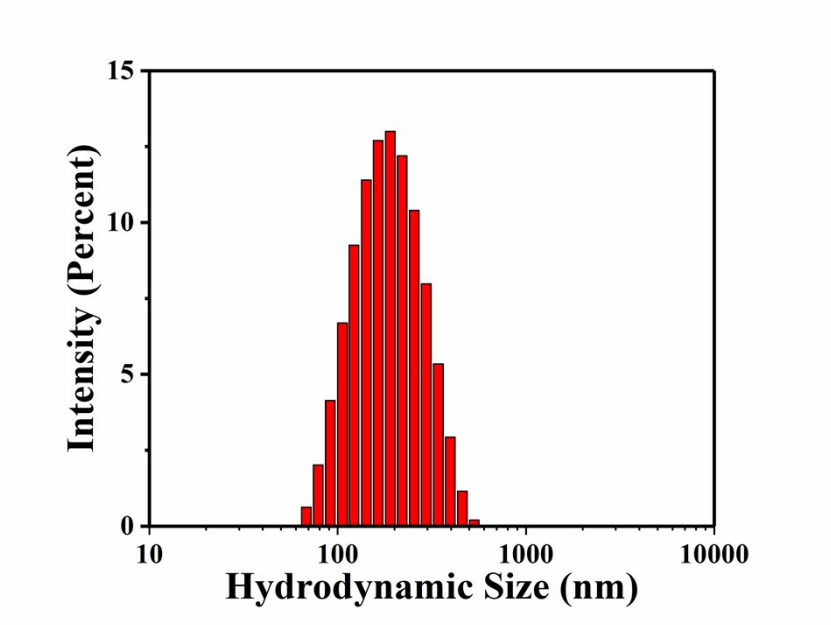

Fig. S5. Hydrodynamic size distribution of Cu(II)Chl-HA NPs.

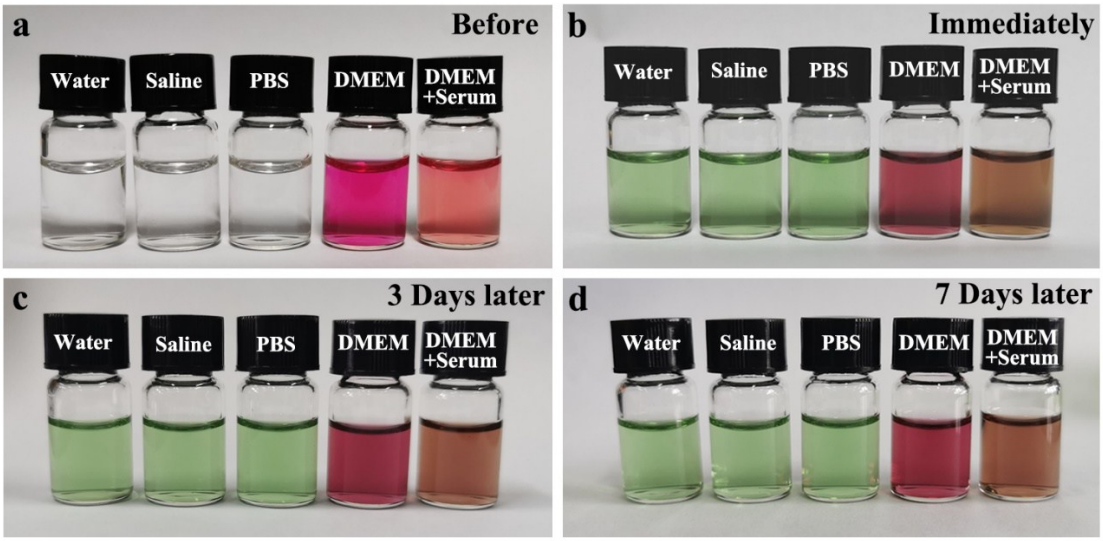

Fig. S6 Time-dependent digital photographs of Cu(II)Chl-HA NPs that dispersed in different media.

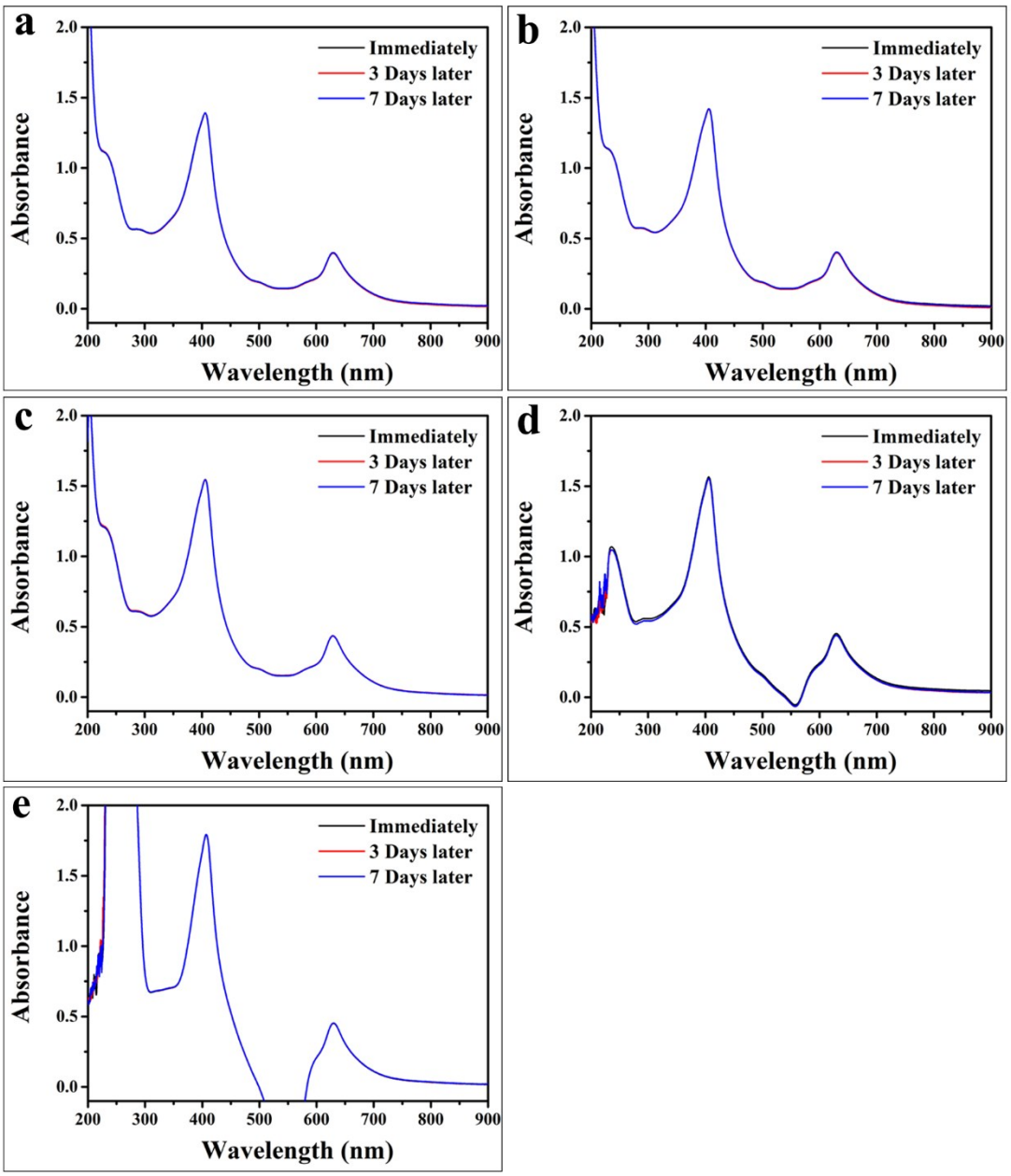

Fig. S7. Time-dependent UV-vis-NIR spectra of Cu(II)Chl-HA NPs that dispersed into (a) water, (b) saline, (c) PBS, (d) DMEM, and (e) DMEM + serum.

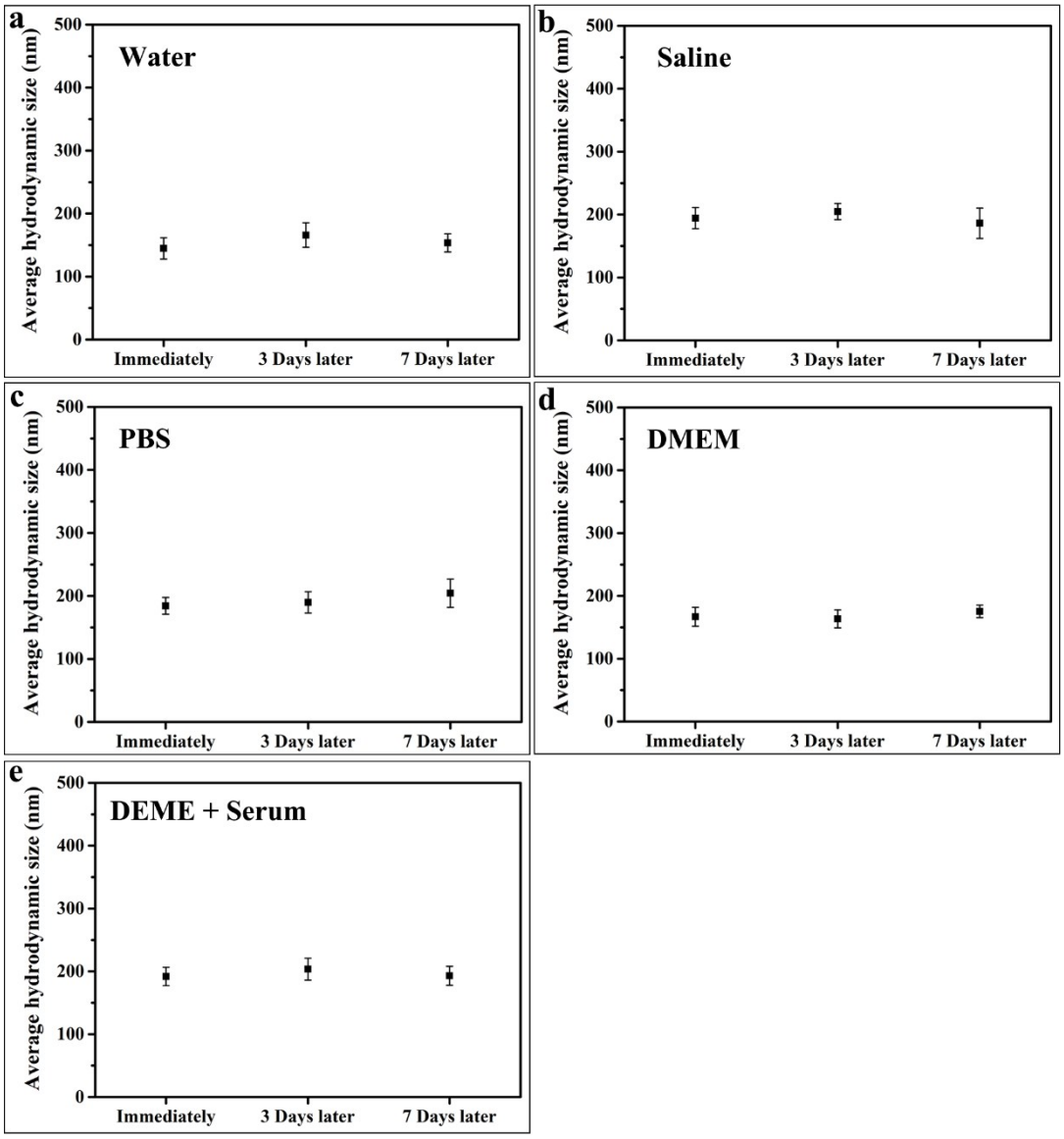

Fig. S8. Time-dependent average hydrodynamic size plots of Cu(II)Chl-HA NPs that dispersed into (a) water, (b) saline, (c) PBS, (d) DMEM, and (e) DMEM + serum.

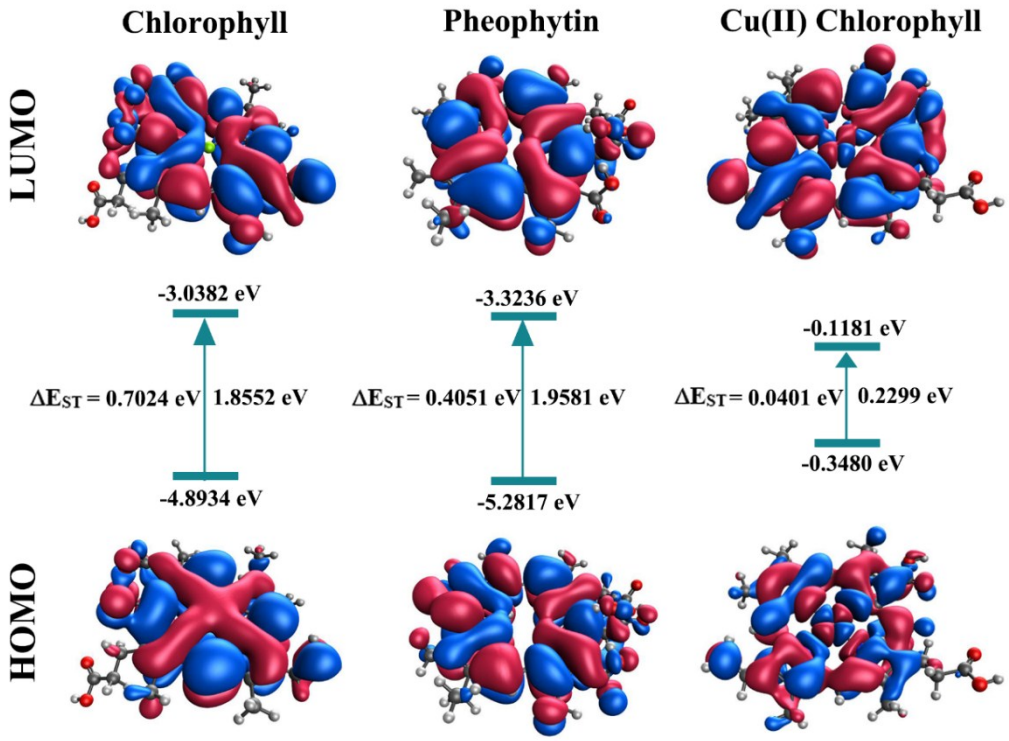

Fig. S9. Frontier molecular orbital distribution of chlorophyll, pheophytin, and Cu(II) Chlorophyll.

Table S1. Triplet and singlet excitation energy of pheophytin, chlorophyll, and Cu(II) chlorophyll calculated by TD-DFT at the B3LYP/6-31G (d) level.

	State	E(eV)	ΔE_{ST}(eV)
Pheophytin	S1	2.1515	0.4051
	S2	2.2812	
	T1	1.7464	
	T2	1.8993	
Chlorophyll	S1	2.1613	0.7024
	S2	2.1706	
	T1	1.4589	
	T2	1.6244	
Cu(II) Chlorophyll	S1	0.6043	0.0401
	S2	0.7155	
	T1	0.5642	
	T2	1.3729	

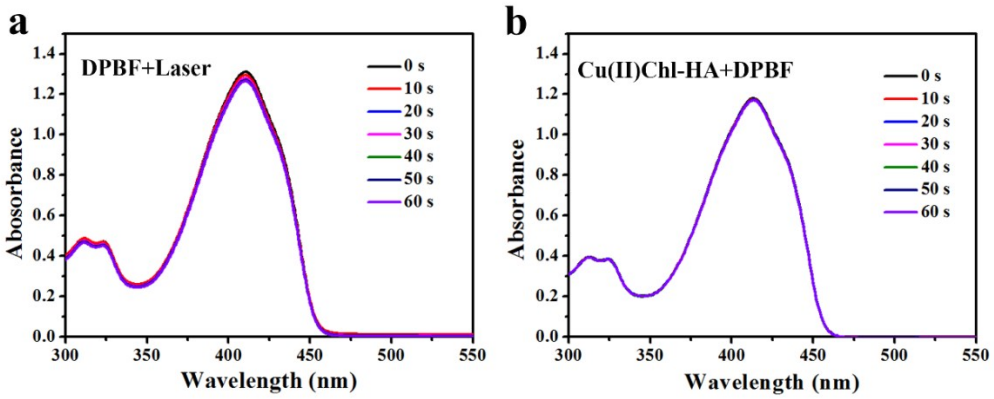

Fig. S10. UV–vis spectra of (a) DPBF + Laser and (b) Cu(II)Chl-HA + DPBF with different irradiation times, respectively.

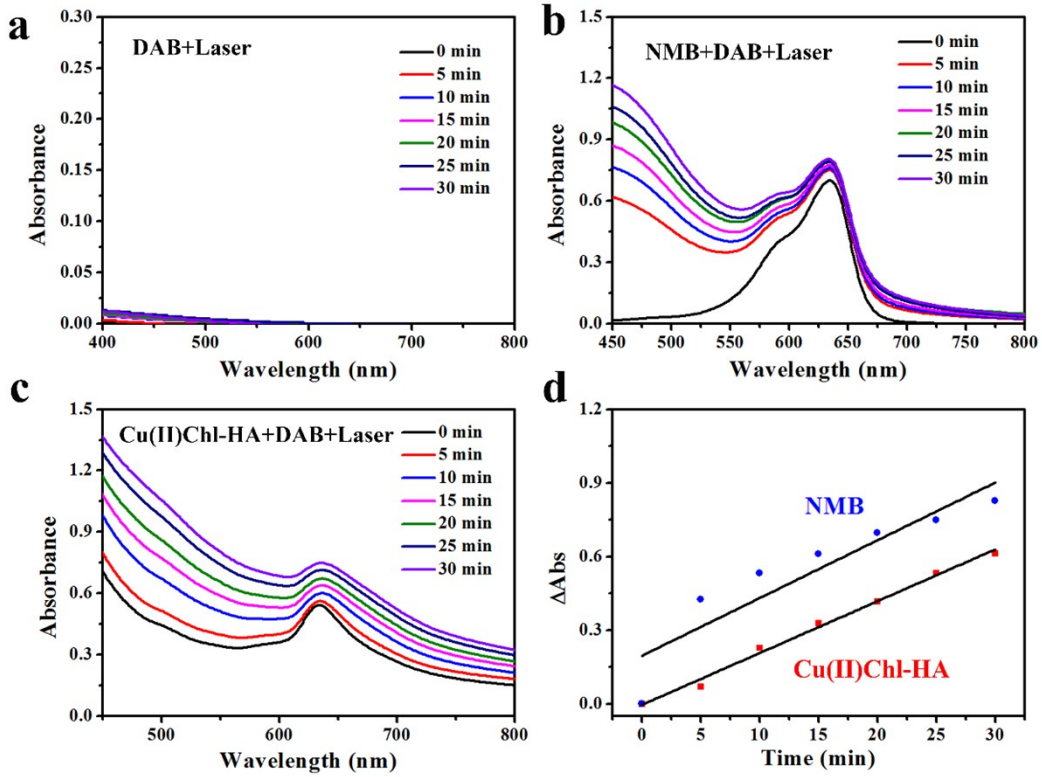

Fig. S11. UV–vis spectra of (a) DAB + Laser, (b) NMB+DAB+Laser, (c) Cu(II)Chl-HA + DAB + Laser with different irradiation times, respectively. (d) The corresponding absorption variations of the DAB solution at 500 nm. [DAB] = 500 μM.

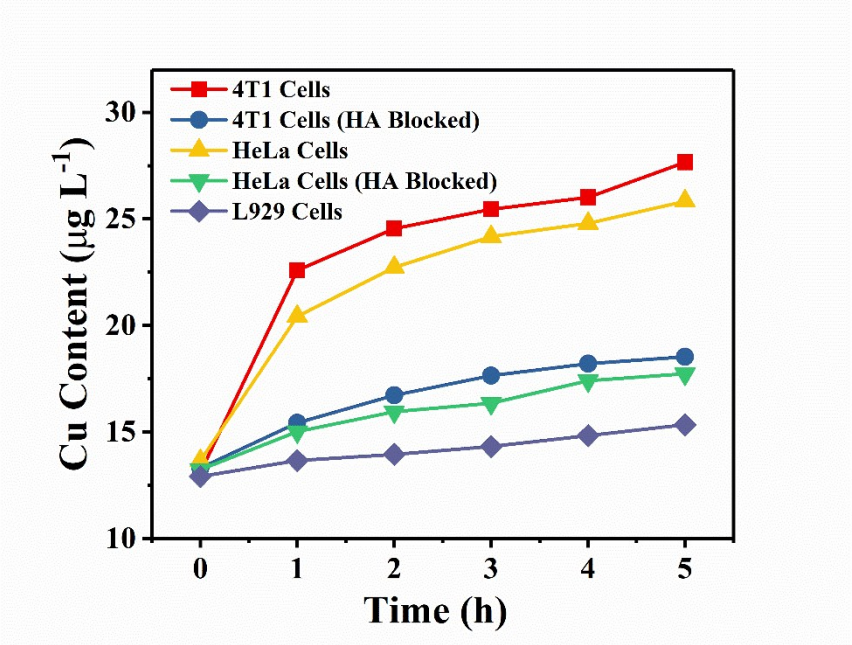

Fig. S12. Time-dependent Cu content of Cu(II)Chl-HA (200 μg mL^{-1}) accumulation in L929, 4T1 and HeLa cells with or without free HA blocked at different incubation time from 0 to 5 h by ICP-OES analysis, respectively.

Table S2. Recent works of power density for photodynamic therapy.

Citations	Substance	Laser	Power density (Note: 1 W = 1 J s)
This work	Cu(II)Chl-HA NPs	650 nm	1.0 W cm^{-2}
Ref 59	HAuNs-p(OEGMAco-MEMA) composites	650 nm	0.75 W cm^{-2}
Ref 60	PC@SWNHs	650 nm	1.0 W cm^{-2}
Ref 61	PDPC micelles	655 nm	2 W cm^{-2}
Ref 62	DAA NPs	660 nm	0.8 W cm^{-2}
Ref 63	PS@chol-BSA NPs	671 nm	1.5 J cm^{-2}
Ref 64	GV-Ce6	671 nm	2 W cm^{-2}

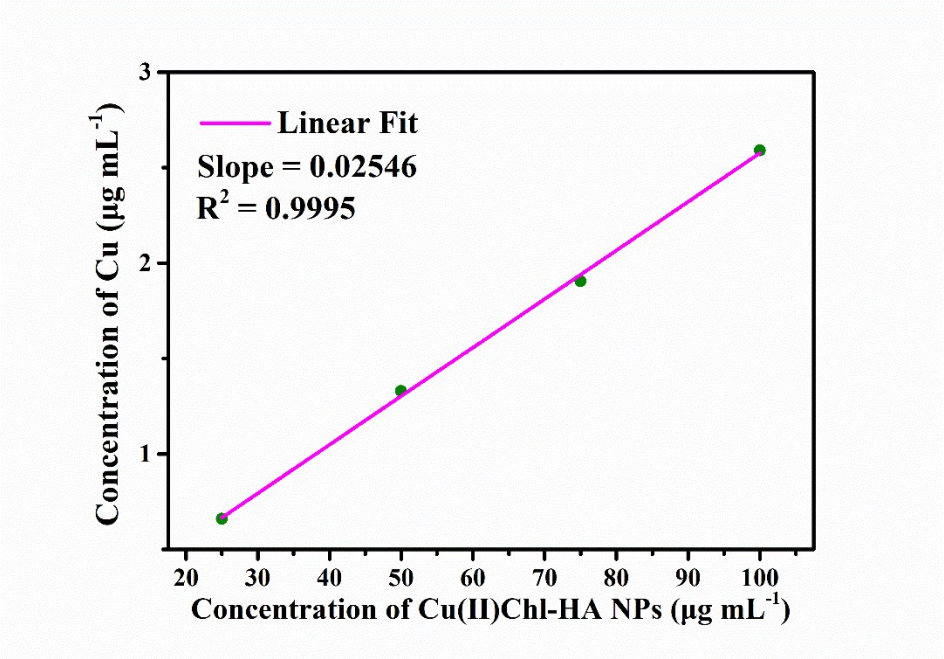

Fig. S13. Plots of Cu contents into Cu(II)Chl-HA NPs with gradient concentration measured by ICP-OES.

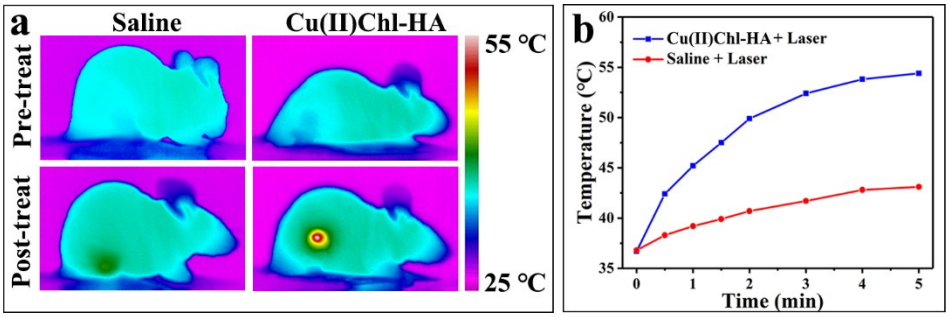

Fig. S14. (a) Digital IR thermal photographs of the 4T1 tumor-bearing mouse after intravenously injection of Cu(II)Chl-HA solution or PBS pre and post irradiation for 5 minutes. (b) Temperature changing curve at solid tumor site in five minutes laser irradiation.

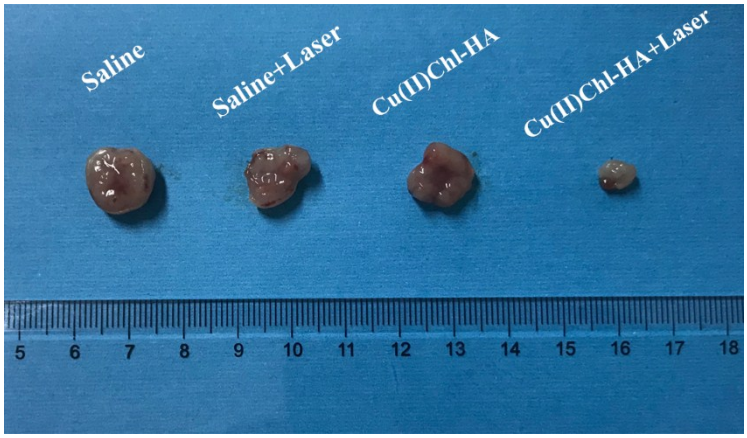

Fig. S15. Digital photograph of representatively harvested tumors.

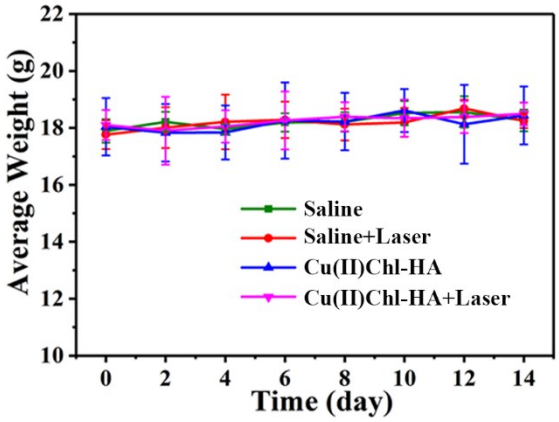

Fig. S16. Average weight changing curve of 4T1 tumor-bearing mouse after different treatments for 14 days.

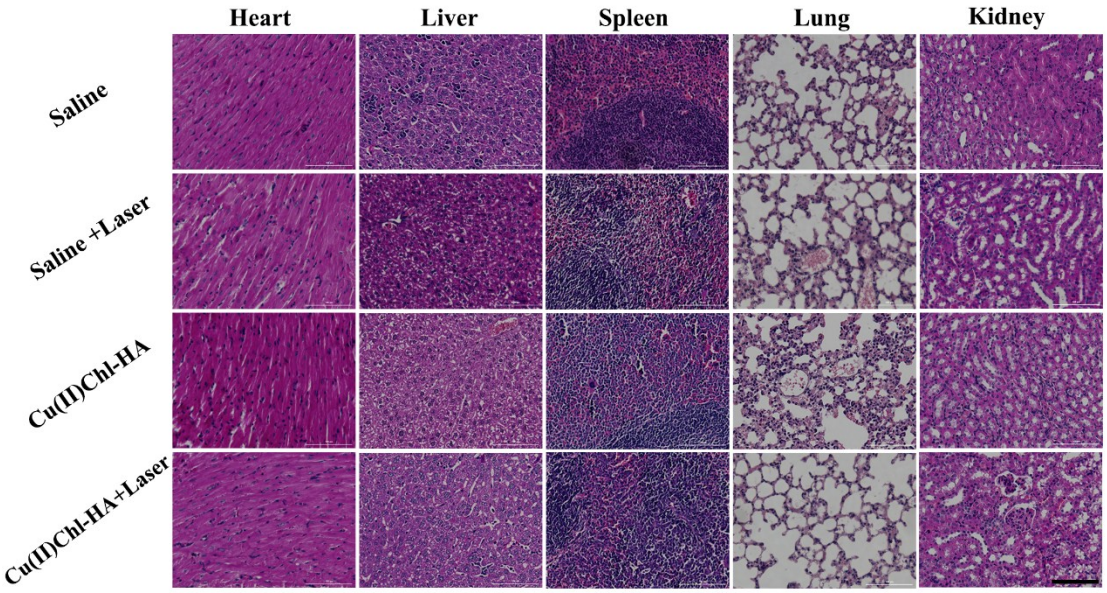

Fig. S17. Histological H&E staining experiment of heart, liver, spleen, lung, and kidney in different condition after 14 days treatments, bar: 100 μm.